Development of Path Integral Monte Carlo Simulations with Localized Nodal Surfaces for Second-Row Elements

Burkhard Militzer[1,2] and Kevin P. Driver[1]
[1]Department of Earth and Planetary Science, University of California, Berkeley 94720, USA
[2]Department of Astronomy, University of California, Berkeley 94720, USA
(Received 11 June 2015; published 22 October 2015)

We extend the applicability range of fermionic path integral Monte Carlo simulations to heavier elements and lower temperatures by introducing various localized nodal surfaces. Hartree-Fock nodes yield the most accurate prediction for pressure and internal energy, which we combine with the results from density functional molecular dynamics simulations to obtain a consistent equation of state for hot, dense silicon under plasma conditions and in the regime of warm dense matter (2.3–18.6 $\mathrm{g\,cm^{-3}}$, $5.0\times10^5-1.3\times10^8$ K). The shock Hugoniot curve is derived and the structure of the fluid is characterized with various pair correlation functions.

DOI: 10.1103/PhysRevLett.115.176403 PACS numbers: 71.15.Mb, 31.15.A-, 61.20.Ja, 64.30.-t

The development of a first-principles methodology for warm dense matter (WDM) applications that treats temperature effects consistently is a key component of the stewardship of plasma science [1,2]. Indeed, technological progress in high energy density physics (HEDP) applications, such as fusion energy [3,4], shock-wave physics [5], astrophysical processes [6–8], and planetary [9,10] and stellar [11] interiors, relies on simulations for input and guidance. WDM is broadly described as the HEDP regime between condensed matter and ideal plasmas, where strong electron correlation and quantum and ionization effects are all important.

For the low-temperature part of the WDM regime, density functional theory molecular dynamics (DFT-MD) [12] is an accurate and efficient first-principles simulation method. The thermal occupation of electronic states is treated as a perturbation of the ground state by Fermi-Dirac smearing [13]. The main drawback of this method is that it becomes computationally infeasible as electrons occupy more bands with increasing temperature. Some alternative DFT-MD-based methods, such as orbital-free DFT [14,15] and average-atom models [16], have made progress on overcoming the thermal-occupation deficiency, but efforts to improve accuracy are still underway [17,18].

Here, we focus on the development of the path integral Monte Carlo (PIMC) method [19], which naturally incorporates finite-temperature quantum effects by working within the many-body thermal density matrix formalism. The combination with Monte Carlo sampling makes this approach one of the most appropriate first-principles simulation techniques for quantum systems at finite temperature (T). Since the length of the path scales as $1/T$, the method becomes increasingly efficient for high temperatures. Electrons and nuclei are often treated equally as paths, but here we treat the nuclei classically because their zero-point motion is negligible for the temperatures under consideration.

PIMC simulations with more than two electrons in a dense system suffer from a fermion sign problem; we solve this by introducing the fixed-node approximation [20,21] that restricts paths so that they remain in the positive regions of a trial density matrix, $\rho_T(\mathbf{R},\mathbf{R}_t;t)>0$. The restricted path integral reads

$$\rho_F(\mathbf{R},\mathbf{R}';\beta)=\frac{1}{N!}\sum_{\mathcal{P}}(-1)^{\mathcal{P}}\int_{\mathbf{R}\to\mathcal{P}\mathbf{R}',\ \rho_T>0}\mathbf{dR}_t e^{-S[\mathbf{R}_t]}, \quad (1)$$

where the action S weights every path and $\mathcal{P}$ denotes permutations of identical particles. The most common approximation to the trial density matrix is a Slater determinant of single-particle density matrices,

$$\rho_T(\mathbf{R},\mathbf{R}';\beta)=\|\rho^{[1]}(r_i,r'_j;\beta)\|_{ij}, \quad (2)$$

in combination with the free-particle (FP) density matrix,

$$\rho_0^{[1]}(r,r';\beta)=\sum_k e^{-\beta E_k}\Psi_k(r)\Psi_k^*(r'), \quad (3)$$

derived from a sum over plane waves, $\Psi_k(r)$. The latter is usually converted into Gaussian form [20]. FP nodes becomes exact in the limit of high temperature. Interaction effects have been introduced to the nodal structure on the variational level [22,23].

In previous work [24–29], we have shown that FP nodes can be sufficient to bridge the WDM regime for elements as heavy as neon. FP nodes work for first-row elements because they can still describe the occupation of the $1s$ state, and DFT-MD works well for lower temperatures where the second shell becomes occupied. In order to simulate second-row elements with PIMC calculations, one must go beyond the FP nodal approximation and incorporate the effects of bound states, as we describe below in an application to silicon.

We chose to study silicon since it is a natural extension of our original work on carbon and is a prototype material

with relevance in the semiconductor industry [30], geophysics and planetary science [10], and astrophysics [11,31–35]. Silicon has a rich solid phase diagram, displaying 11 solid-state phases under pressure and becoming metallic near 12 GPa [36–38]. A number of dynamic shock compression experiments have been performed [39–45]. Shock-compressed silicon has been studied theoretically with several classical [46–49] and one DFT-MD simulation [50] that investigated pressures up to 500 GPa and temperatures up to 10^4 K. Dynamical properties of shocked silicon plasma states have also been studied extensively by theoretical approaches [51–55].

We perform standard DFT-MD simulations using the VASP code [56]. Supercells with 8 atoms were used for $T \geq 2.5 \times 10^5$ K, where the kinetic energy far outweighs the interaction energy, and cells with 24 atoms were used at lower temperatures [29]. Additional details are provided in the Supplemental Material [57]. For the PIMC calculations, we have used our own code, CUPID [61]. The Coulomb interaction is introduced through pair density matrices [62–64]. The nodes are enforced at intervals of 1/8192 Hartrees (Ha), which means we need between 4 and 2560 time slices for simulations in the temperature range of $129 - 1 \times 10^6$ K. It is sufficient to evaluate the pair action only at intervals of 1/1024 Ha [23].

We began our investigation of localized nodal approximations in PIMC calculations with the relatively simple, proof-of-concept problem of computing internal energy and pressure of a stationary silicon atom (one nucleus and 14 electrons) in a periodic cell over a wide temperature range. In Fig. 1, we compared energies from DFT and PIMC calculations using FP nodes, where we found a discrepancy of 5.2 Ha at 2×10^6 K that increased to 12.6 Ha at 5×10^5 K. We attributed this discrepancy primarily to the FP nodal approximation, which, as we have shown, works well only as long as the second shell is not significantly occupied [27].

We investigated two approaches to improve upon the FP nodal approximation. First, we added the bound eigenstates of the Coulomb potential of the silicon nuclei, $\Psi_s(r - R_I)$, to the nodal approximation in Eq. (3),

$$\rho^{[1]}(r, r', \beta) = \sum_{I=1}^{N} \sum_{s=0}^{n} e^{-\beta E_s} \Psi_s(r - R_I) \Psi_s^*(r' - R_I), \quad (4)$$

where the number of states n needs to be at least 7 in each spin channel in order to provide at least one bound state for every electron. We used the efficient formulation of the Coulomb density matrix put forth in Ref. [62] and, hence, we refer to these nodes as Pollock nodes. The $1s$ state ($n = 1$) has been added to PIMC nodes once before to simulate dense hydrogen [65]; agreement with DFT predictions and experimental results was, however, not as good as expected because additional approximations were introduced when the nodes were enforced. Here we enforce the nodes strictly as outlined in Refs. [20,21].

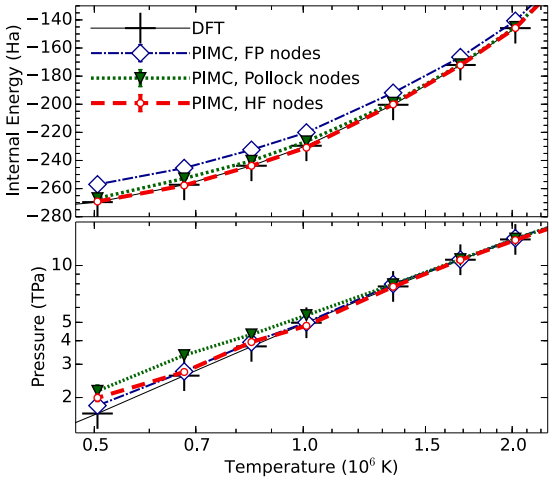

FIG. 1 (color online). Internal energy and pressure vs temperature for a single silicon atom in periodic cell of 5.0 Bohr.

The adoption of Pollock nodes reduced the energy deviation between DFT and PIMC calculations from 12.6 to 2.7 Ha at 5×10^5 K. However, the pressure deviations increased from 11% to 31% (Fig. 1). We tried to improve this result by varying the number of bound states in Eq. (4), testing different time steps, studying various numbers of electrons, and, finally, by developing a multideterminantal nodal surface in the spirit of quantum chemistry. In the multideterminantal approach, we adopted a sum of FP fermion determinants where each is added to a different bound shell with the appropriate $e^{-\beta E_s}$ weight. However, this approach did not lead to a significant improvement in the predicted pressure. This discrepancy led us to abandon the Pollock node approximation. We concluded that the eigenstates of noninteracting particles in the Coulomb potential are too confining for interacting electrons.

In our second approach, we constructed a thermal density matrix from Hartree-Fock (HF) orbitals that we computed with the GAMESS code [66] and expanded in a localized basis set (6-31 + +G). We again used Eq. (4), but this time the functions $\Psi_s(r)$ become the HF orbitals, which are weighted by factors $e^{-\beta E_s}$ where E_s is set to the corresponding HF eigenvalue. Our approach differs from ground state HF nodes [67]. With our HF nodal approximation, we found perfect agreement with the DFT prediction for the internal energy of the silicon atom over the entire temperature range under consideration (Fig. 1). The resulting PIMC energies are consistently lower than those obtained with the other two nodal approximations, which, as illustrated in the Supplemental Material [57], implies a lower free energy [23] and establishes HF nodes as the most accurate nodes among the three approximations considered here. The PIMC pressures derived with HF nodes agree

within the 1σ error bars for all temperatures of 7×10^5 K and higher. For 5×10^5 K, a small pressure discrepancy remained, but, given the large improvement over FP and Pollock nodes, we decided to adopt HF nodes for the many-particle simulations with moving nuclei that we discuss for the remainder of this Letter.

The evaluation of HF orbitals for many moving particles adds a non-negligible burden to the computation of the nodes. We vectorized this part of the calculation by evaluating the orbitals for many positions at once. We updated the inverse of the determinants whenever possible rather than recomputing it. Nevertheless, when one ion is moved, all determinants need to be reevaluated; this is not the case for FP nodes, which are independent of the ion positions. Despite this additional cost, we were able to perform PIMC simulations with 8 nuclei and 112 electrons for temperatures of 1×10^6 K and above.

We needed to introduce one more methodological development. Upon introducing HF nodes into our simulations with moving nuclei, the acceptance ratio of the ion moves rapidly decayed to zero at lower and intermediate temperatures as electron paths began to sample the bound states at the nuclei. Because the nodal surfaces now depend on the nuclear positions, node crossings are almost unavoidable when an ion is moved. The crossing is almost exclusively triggered by nearby electrons. The decay in efficiency was so detrimental that we could not have obtained the smooth $g(r)$ functions in Fig. 2 without the development of multiparticle moves that relocate one nucleus and nearby electrons at once. We needed to design an algorithm that satisfied the detailed balance requirement [19] and did not rely on any permanent pairing of electrons and ions. We introduced a localization function,

$$L_{Ij} = \int_0^\beta dt |\Psi_{1s}(r_j(t) - R_I)|^2, \tag{5}$$

that assigns a probability of finding electron paths, $r_j(t)$, near ion I. Adopting concepts from the permutation sampling in Ref. [19], we multiply these probabilities to construct a table that contains all moves of one ion with up to four electron paths, including those that permute. Because L_{Ij} is a very localized function, the number of significant entries is fairly small; the table can thus be constructed efficiently. Once a particular move has been selected from the table, we shift the entire group to a new location within a box of 0.5 Bohr without otherwise changing their paths. This leaves the function L_{Ij} unchanged within the group, which means that the detailed balance can be satisfied by adopting a particularly simple expression for the acceptance ratio: the sum of the table entries for the new location divided by that for the original coordinates. This procedure leads to very efficient ion moves. To change the internal coordinates of electron paths, we continue to rely on the single- and multielectron moves [19].

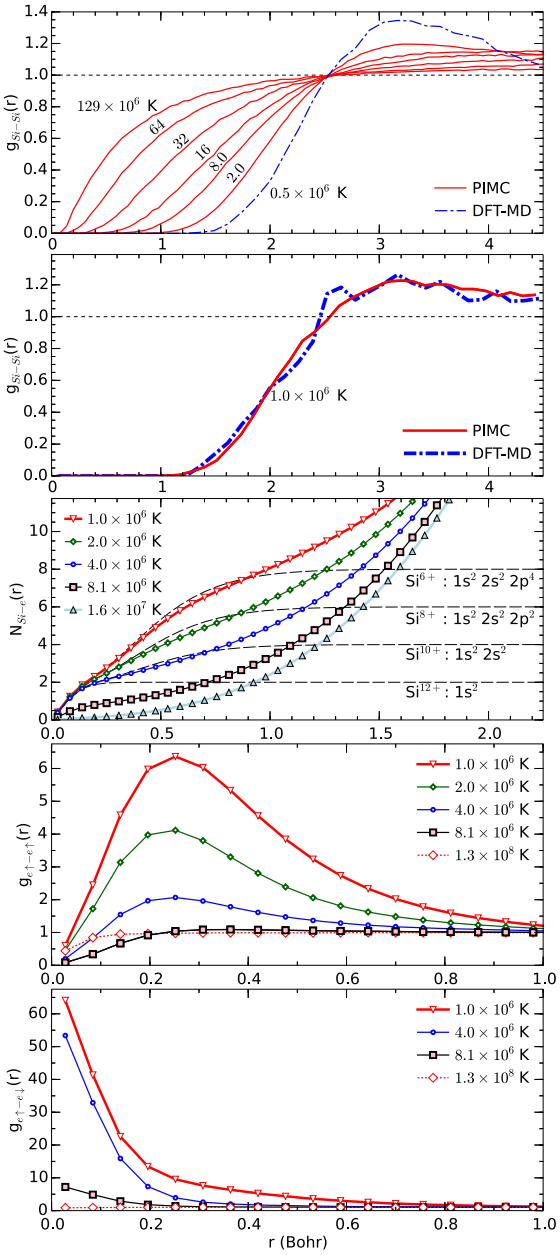

FIG. 2 (color online). The top two panels compare the nuclear pair correlation functions from PIMC calculations and DFT-MD at various temperatures. The middle panel shows the integrated nucleus-electron pair correlation function, $N(r)$, computed with PIMC calculations. Results are compared with an isolated ion in order to estimate the ionization state of the plasma. The two lowest panels display the electron-electron pair correlation functions for pairs with parallel and opposite spins. All results are for fourfold compression.

Figure 3 and Supplemental Table S1 [57] summarize our equation-of-state calculations. For the density interval of onefold to eightfold the ambient density of 2.329 g cm^{-3}, PIMC simulations with HF nodes were performed for a temperature range of $129 - 2 \times 10^6$ K and DFT-MD simulations for $2 - 0.05 \times 10^6$ K. At 2×10^6 K, both methods

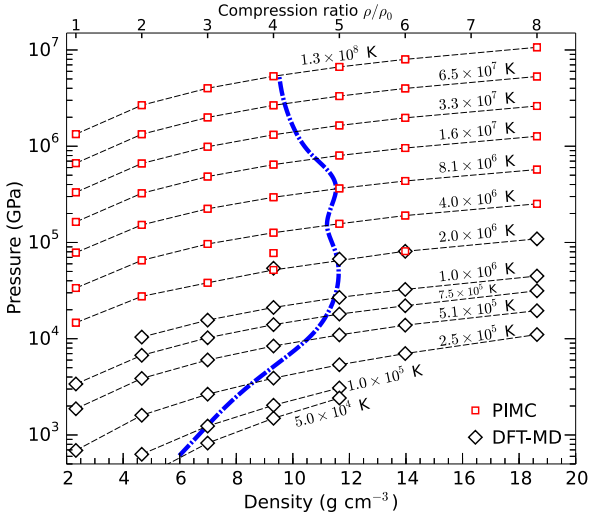

FIG. 3 (color online). Pressure-density conditions of our PIMC and DFT-MD simulations. The blue line shows the shock Hugoniot curve.

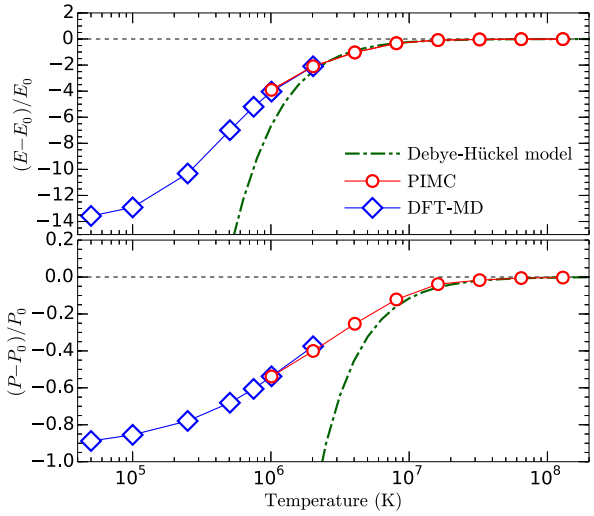

FIG. 4 (color online). Internal energy and pressure for a silicon plasma at a density of 9.316 g cm^{-3} are shown vs temperature. We plot the excess quantities relative to a fully ionized non-interacting plasma.

yield consistent thermodynamic and structural properties despite the fact that both techniques involve very different concepts and approximations. The predicted internal energies deviate by up to 5 Ha/atom and the pressure by up to 4%. A difference of 5 Ha/atom would be equivalent to a 2.5% difference in the ionization fraction of the second shell. We attribute these deviations to a combined effect of three approximations: the ground state DFT exchange-correlation functional, the frozen-core DFT pseudopotential, and our localized nodes in PIMC calculations. While it is difficult to disentangle the errors due to these approximations, we anticipate that the discrepancies will be further reduced when both methods are improved in the future. Figure 4 illustrates that the deviations between PIMC calculations and DFT-MD are small compared to the error in the Debye model. We only plotted excess quantities relative to a fully ionized plasma model because the total internal energy varies by over 10 000 Ha/atom in the parameter range of consideration.

Good agreement between PIMC calculations and DFT-MD is found for the nuclear pair correlation shown in Fig. 2. With PIMC calculations, we were also able to derive the integrated nucleus-electron pair correlation function, $N(r)$, that measures how many electron reside on average within a radius r from a nucleus. Comparing the information at small r with results for isolated ions, we can estimate the degree of ionization in the plasma. For temperatures of 1, 2, and 4×10^6 K, we estimate the average charge of the silicon ions to be +6, +8, and +10 respectively. At higher temperature, the $1s$ states becomes partially ionized as well.

The electron-electron pair correlation functions in Fig. 2 yield strong positive correlations, which underlines the fact that multiple electrons are bound to one nucleus. As the temperature is increased, the positive correlation diminishes and, eventually, even the negative correlations between electrons with parallel spins at small r are reduced.

Finally, we derive the principal shock Hugoniot curve [68]. Under shock compression, a material changes from an initial state with internal energy, pressure, and volume ($E_0 = -289.166$ Ha/atom, $P_0 = 1$ bar, V_0 from $\rho_0 = 2.329$ g cm^{-3}) to a final state denoted by (E, P, V) that we can predict theoretically. The shock compression ratio, ρ/ρ_0, is controlled by interaction effects and by excitations of internal degrees of freedom. In Fig. 3, a maximum compression ratio of 4.99 is reached for 1.6×10^6 K where approximately 7 of 14 electrons have been ionized. A second compression maximum of 4.95 is predicted to occur at 8.3×10^6 K, which is caused by the ionization of the $1s$ state. As we have seen for neon [29], the temperature is too high for this maximum to be studied with DFT-MD. Therefore, a combined PIMC and DFT-MD approach is needed to study all features of the principal Hugoniot curve.

By constructing a thermal density matrix with HF orbitals for the purpose of computing fermion nodes, we were able to perform PIMC simulations with heavier elements than previously possible. Through the optimized evaluation of such nodes and the adoption of multiparticle Monte Carlo moves, we were able to put together an efficient algorithm and derive the equation of state of silicon plasmas. At lower temperatures, we add results from standard DFT-MD simulations. By combining both techniques, we provide a first-principles treatment for all second-row elements in the regime of warm dense matter and for plasma conditions.

This research is supported by the DOE (Grant No. DE-SC0010517). Computational support was provided by NASA, NERSC, and NCAR. B. Austin provided support for reading in the GAMESS orbitals. J. Demmel gave advice on the numerics of determinant evaluations.

[1] *Advancing the Science of High Energy Density Laboratory Plasmas*, edited by R. Betti (Office of Fusion Energy Science (OFES)/Fusion Energy Science Advisory Committee (FESAC), Washington, DC, 2009).

[2] *Basic Research Needs for High Energy Density Laboratory Physics*, edited by R. Rosner, D. Hammer, and T. Rothman (U.S. Department of Energy, Washington, DC, 2009).

[3] M. K. Matzen, M. A. Sweeney, R. G. Adams, J. R. Asay, J. E. Bailey, G. R. Bennett, D. E. Bliss, D. D. Bloomquist, T. A. Brunner, R. B. Campbell *et al.*, Phys. Plasmas **12**, 055503 (2005).

[4] I. Cook, Nat. Mater. **5**, 77 (2006).

[5] R. Cauble, D. K. Bradley, P. M. Celliers, G. W. Collins, L. B. D. Siliva, and S. J. Moon, Contrib. Plasma Phys. **41**, 239 (2001).

[6] H. M. V. Horn, Science **252**, 384 (1991).

[7] G. Chabrier, F. Douchin, and A. Y. Potekhin, J. Phys. Condens. Matter **14**, 9133 (2002).

[8] M. Cotelo, P. Velarde, A. G. de la Varga, and C. Garcia-Fernandez, Astrophys. Space Sci. **336**, 53 (2011).

[9] J. J. Fortney, S. H. Glenzer, M. Koenig, B. Militzer, D. Saumon, and D. Valencia, Phys. Plasmas **16**, 041003 (2009).

[10] A. Bennuzzi-Mounaix, S. Mazevet, A. Ravasio, T. Vinci, A. Denoeud, M. Koenig, N. Amadou, E. Brambrink, F. Festa, A. Levy *et al.*, Phys. Scr. **T161**, 014060 (2014).

[11] C. Hansen and S. Kawaler, *Stellar Interiors: Physical Principles, Structure, and Evolution*, Astronomy and Astrophysics Library Vol. 1 (Springer-Verlag, New York, 1994).

[12] D. Marx and J. Hutter, in *Modern Methods and Algorithms of Quantum Chemistry*, edited by Johannes Grotendorst, NIC Series Vol. 1 (John-von-Neumann-Inst. for Computing, Forschungszentrum Jülich, Germany, 2000), p. 301.

[13] M. Verstraete and X. Gonze, Phys. Rev. B **65**, 035111 (2001).

[14] F. Lambert, J. Clérouin, and S. Mazevet, Europhys. Lett. **75**, 681 (2006).

[15] F. Lambert, J. Clérouin, S. Mazevet, and D. Gilles, Contrib. Plasma Phys. **47**, 272 (2007).

[16] B. F. Rozsnyai, High Energy Density Phys. **10**, 16(2014).

[17] V. V. Karasiev, D. Chakraborty, O. A. Shukruto, and S. B. Trickey, Phys. Rev. B **88**, 161108 (2013).

[18] T. Sjostrom and J. Daligault, Phys. Rev. Lett. **113**, 155006 (2014).

[19] D. M. Ceperley, Rev. Mod. Phys. **67**, 279 (1995).

[20] D. M. Ceperley, J. Stat. Phys. **63**, 1237 (1991).

[21] D. M. Ceperley, in *Monte Carlo and Molecular Dynamics of Condensed Matter Systems*, edited by E. K. Binder and G. Ciccotti (Editrice Compositori, Bologna, Italy, 1996).

[22] B. Militzer and E. L. Pollock, Phys. Rev. E **61**, 3470 (2000).

[23] B. Militzer and D. M. Ceperley, Phys. Rev. Lett. **85**, 1890 (2000).

[24] B. Militzer, D. M. Ceperley, J. D. Kress, J. D. Johnson, L. A. Collins, and S. Mazevet, Phys. Rev. Lett. **87**, 275502 (2001).

[25] B. Militzer, Phys. Rev. Lett. **97**, 175501 (2006).

[26] B. Militzer, Phys. Rev. B **79**, 155105 (2009).

[27] K. P. Driver and B. Militzer, Phys. Rev. Lett. **108**, 115502 (2012).

[28] L. X. Benedict, K. P. Driver, S. Hamel, B. Militzer, T. Qi, A. A. Correa, A. Saul, and E. Schwegler, Phys. Rev. B **89**, 224109 (2014).

[29] K. P. Driver and B. Militzer, Phys. Rev. B **91**, 045103 (2015).

[30] G. J. Cheng, M. Cai, D. Pirzada, M. J.-F. Guinel, and M. G. Norton, J. Manuf. Sci. Eng. **130**, 011008 (2008).

[31] E. Herbst, T. Millar, S. Wlodek, and D. Bohme, Astron. Astrophys. **222**, 205 (1989).

[32] W. D. Langer and A. E. Glassgold, Astrophys. J. **352**, 123 (1990).

[33] D. D. S. MacKay, Mon. Not. R. Astron. Soc. **274**, 694 (1995).

[34] P. Schilke, C. M. Walmsley, G. Pineau des Forets, and D. R. Flower, Astron. Astrophys. **321**, 293 (1997).

[35] A. P. Jones, A. G. G. M. Tielens, D. J. Hollenbach, and C. F. Mckee, Astrophys. J. **433**, 797 (1994).

[36] A. Mujica, A. Rubio, A. Muñoz, and R. J. Needs, Rev. Mod. Phys. **75**, 863 (2003).

[37] D. Alfè, M. J. Gillan, M. D. Towler, and R. J. Needs, Phys. Rev. B **70**, 214102 (2004).

[38] R. G. Hennig, A. Wadehra, K. P. Driver, W. D. Parker, C. J. Umrigar, and J. W. Wilkins, Phys. Rev. B **82**, 014101 (2010).

[39] P. Celliers, A. Ng, G. Xu, and A. Forsman, Phys. Rev. Lett. **68**, 2305 (1992).

[40] R. R. Alcon, D. L. Robbins, S. A. Sheffield, D. B. Stahl, and J. N. Fritz, AIP Conf. Proc. **706**, 651 (1977).

[41] S. Gilev and A. Trubachev, Phys. Status Solidi B **211**, 379 (1999).

[42] S. D. Gilev and A. M. Trubachev, J. Phys. Condens. Matter **16**, 8139 (2004).

[43] T. Löwer, V. N. Kondrashov, M. Basko, A. Kendl, J. Meyer-ter Vehn, R. Sigel, and A. Ng, Phys. Rev. Lett. **80**, 4000 (1998).

[44] A. Loveridge-Smith, A. Allen, J. Belak, T. Boehly, A. Hauer, B. Holian, D. Kalantar, G. Kyrala, R. W. Lee, P. Lomdahl *et al.*, Phys. Rev. Lett. **86**, 2349 (2001).

[45] H. Kishimura, H. Matsumoto, and N. N. Thadhani, J. Phys. Conf. Ser. **215**, 012145 (2010).

[46] G. Mogni, A. Higginbotham, K. Gaál-Nagy, N. Park, and J. S. Wark, Phys. Rev. B **89**, 064104 (2014).

[47] E. J. Reed, AIP Conf. Proc. **620**, 343 (2002).

[48] Z. Li, D. Chen, J. Wang, and L. Shao, J. Appl. Phys. **115**, 143507 (2014).

[49] I. I. Oleynik, S. V. Zybin, M. L. Elert, and C. T. White, AIP Conf. Proc. **845**, 413 (2006).

[50] D. C. Swift, G. J. Ackland, A. Hauer, and G. A. Kyrala, Phys. Rev. B **64**, 214107 (2001).

[51] A. Ng, P. Celliers, G. Xu, and A. Forsman, Phys. Rev. E **52**, 4299 (1995).

[52] A. Ng, AIP Conf. Proc. **620**, 53 (2002).

[53] A. Ng, Int. J. Quantum Chem. **112**, 150 (2012).

[54] J. Vorberger, D. O. Gericke, T. Bornath, and M. Schlanges, Phys. Rev. E **81**, 046404 (2010).

[55] J. Vorberger, Z. Donko, I. M. Tkachenko, and D. O. Gericke, Phys. Rev. Lett. **109**, 225001 (2012).

[56] G. Kresse and J. Furthmüller, Phys. Rev. B **54**, 11169 (1996).

[57] See Supplemental Material at http://link.aps.org/supplemental/10.1103/PhysRevLett.115.176403, which includes Refs. [58–60].

[58] J. P. Perdew, K. Burke, and M. Ernzerhof, Phys. Rev. Lett. **77**, 3865 (1996).

[59] E. W. Brown, B. K. Clark, J. L. DuBois, and D. M. Ceperley, Phys. Rev. Lett. **110**, 146405 (2013).

[60] P. E. Blöchl, Phys. Rev. B **50**, 17953 (1994).
[61] B. Militzer, Ph.D. thesis, University of Illinois at Urbana-Champaign, 2000.
[62] E. L. Pollock, Comput. Phys. Commun. **52**, 49 (1988).
[63] V. Natoli and D. M. Ceperley, J. Comput. Phys. **117**, 171 (1995).
[64] B. Militzer and R. L. Graham, J. Phys. Chem. Solids **67**, 2136 (2006).
[65] S. A. Khairallah, J. Shumway, and E. Draeger, arXiv: 1108.1711.
[66] M. W. Schmidt, K. K. Baldridge, J. A. Boatz, S. T. Elbert, M. S. Gordon, J. J. Jensen, S. Koseki, N. Matsunaga, K. A. Nguyen, S. Su *et al.*, J. Comput. Chem. **14**, 1347 (1993).
[67] J. Shumway, in *Computer Simulation Studies in Condensed-Matter Physics XVI* (Springer, Berlin Heidelberg, 2006), p. 181.
[68] Y. B. Zeldovich and Y. P. Raizer, *Elements of Gasdynamics and the Classical Theory of Shock Waves* (Academic Press, New York, 1968).